PASJ: Publ. Astron. Soc. Japan , 1–??,

Secular Evolution of Barred Galaxies with Massive Central Black Holes

Shunsuke HOZUMI
Faculty of Education, Shiga University, 2-5-1 Hiratsu, Otsu, Shiga 520-0862
hozumi@sue.shiga-u.ac.jp
and
Lars HERNQUIST
Harvard-Smithsonian Center for Astrophysics, 60 Garden Street, Cambridge, MA 02138, U.S.A.
lars@cfa.harvard.edu

(Received 2004 September 10; accepted 2005 July 12)

Abstract

The influence of central black holes on the dynamical evolution of bars in disk galaxies was examined. Once a bar formed by a dynamical instability in an infinitesimally thin stellar disk was fully developed, a black hole (BH) was adiabatically added at the center of the disk. Our results indicate that a bar can be completely destroyed, in a practical sense, in a time much smaller than the Hubble time if the central BH mass exceeds about 0.5% of the disk mass. Since this implied minimum BH mass for bar destruction is on the order of $10^{8.5}M_\odot$ for a typical disk galaxy, this process could occur in the real Universe. The bar amplitude decreases gradually with time after the BH has grown up to its full mass. Surface-of-section plots indicate that the bar dissolution originates from the chaotic behavior of bar-supporting orbits. In addition, the scale-length and the radial velocity dispersion of the disk after bar dissolution become much larger than those of the initial axisymmetric disk. This finding suggests that it is possible to discriminate between genuine non-barred galaxies and bar-dissolved galaxies induced by massive central BHs from the viewpoint of structural properties.

Key words: black hole physics — galaxies: evolution — galaxies: kinematics and dynamics — galaxies: structure — methods: n-body simulations

1. Introduction

Observations indicate that massive central black holes exist in disk galaxies as well as in ellipticals. It is also thought that the black hole masses are correlated with host galaxy properties; Kormendy and Gebhardt (2001) have concluded that the median black hole (BH) mass fraction is 0.13% of the mass of the bulge, where the term "bulge" is used for the hot spheroidal component of a host galaxy. Consequently, extremely massive central BHs are more frequently observed in elliptical and S0 galaxies than in normal spirals. For example, NGC 3115 (type S0), NGC 4649 (type E1), and M 87 (type E0) are thought to harbor central BHs with masses of $9.1\times10^8M_\odot, 2.0\times10^9M_\odot$, and $3.4\times10^9M_\odot$, respectively, while NGC 4945 (type Scd), the Milky Way (type SBbc), NGC 1068 (type Sb), NGC 4258 (type Sbc), M 31 (type Sb), and NGC 4594 (type Sa) are believed to contain BHs with masses of $1.4\times10^6M_\odot, 1.8\times10^6M_\odot, 1.5\times10^7M_\odot, 3.9\times10^7M_\odot, 4.5\times10^7M_\odot$, and $1.0\times10^9M_\odot$, respectively (see, e.g., Kormendy, Gebhardt 2001; Tremaine et al. 2002; Marconi, Hunt 2003; and references therein). It is thus plausible that most, if not all, large galaxies contain central black holes whose masses range from $\sim10^6M_\odot$ to $\sim10^{9.5}M_\odot$.

Such a large mass concentration at the center of a galaxy could affect the structure of the entire system. Of great interest is the influence of a central BH on the structure of a bar, in view of the fact that more than two-thirds of all disk galaxies are barred if we include weakly barred galaxies in addition to strongly barred galaxies (Eskridge et al. 2000). Hasan and Norman (1990) and Hasan, Pfenniger, and Norman (1993) have shown that central mass concentrations can destroy a bar within a short period of time based on the orbital motions of test particles in fixed potentials of a disk, bar, and black hole. Subsequently, Norman, Sellwood, and Hasan (1996) and Shen and Sellwood (2004) have demonstrated that central mass concentrations can also dissolve a self-consistent bar by carrying out N-body simulations in which a bar is generated by the bar instability as a natural product of self-gravitating disks, and a BH is added at the center of the disk as an external field. From their self-consistent simulations, Norman et al. (1996) have concluded that a central massive object with about 5% of the total mass of a disk plus bulge can result in the dissolution of a bar within the Hubble time. Likewise, Shen and Sellwood (2004) obtained about 4–5% of the disk mass as a minimum BH mass necessary for bar dissolution. Although these results are intriguing, the implied mass for bar destruction becomes about $10^{9.5}M_\odot$ when scaled to a typical disk galaxy with a mass of $\sim10^{10.5}$–$10^{11}M_\odot$. Consequently, the required BH mass is greater than that inferred in nearby spirals, and is comparable to the largest BH masses derived observationally in ellipticals.

It follows from the argument mentioned above that

bar destruction by massive central black holes might not practically occur in the real Universe. However, the conclusions of Norman et al. (1996) and Shen and Sellwood (2004) have been reached by employing Kuzmin–Toomre disks (Kuzmin 1956; Toomre 1963), which differ from the mass profiles of real disk galaxies, which are well-represented by exponential surface density profiles (Freeman 1970). Since exponential disks are more centrally concentrated than Kuzmin–Toomre disks, central BHs may have a more serious effect on exponential disks than on Kuzmin–Toomre disks. Thus, the minimum BH mass could be smaller than that obtained by Norman et al. (1996) and that by Shen and Sellwood (2004). Therefore, it is important to determine how massive a BH is required to destroy a bar for realistic disk models. In fact, our results for exponential disks will demonstrate that in some cases the BH mass necessary for bar destruction may be at least a factor of ten smaller than that suggested by the work of those authors noted above. This implies that a bar could be dissolved in reality, so it is also important to study the structural properties of bar-dissolved galaxies in order to observationally discriminate them from a priori non-barred galaxies.

In this paper, we examine the influence of a central black hole on a bar generated by the bar instability, and show that the BH mass necessary for bar destruction could be within the largest BH masses observed in nearby spirals. Then, we study what structural properties bar-dissolved galaxies have, and describe ways of discriminating between bar-dissolved galaxies and genuine non-barred galaxies. In section 2, we present the initial setup of our models and the numerical method. Results are given in section 3. In section 4, we discuss the BH mass required for bar dissolution, and the structural characteristics of bar-dissolved galaxies, together with the mechanism of bar dissolution studied here. Conclusions are given in section 5.

2. Models and Method

In the calculations described here, we study the evolution of razor-thin disks without bulges and halos. Since the surface density profile of disk galaxies is well-described by an exponential law (Freeman 1970), we adopt exponential disks whose surface density distributions, μ, are given by

$$\mu(R) = \mu_0 \exp(-R/h), \tag{1}$$

where h is the scale-length, R is the distance from the center of the disk, and μ_0 is the surface density at the center. The disks are truncated at $R = 10h$. The full phase-space is realized by employing the approach of Hernquist (1993), who approximated the velocity distribution using moments of the collisionless Boltzmann equation. The shape of the velocity ellipsoid in this approach is based on observations (van der Kruit, Searle 1981; Lewis, Freeman 1989) such that the square of the radial velocity dispersion, ${\sigma_r}^2$, is proportional to the surface density, and so, ${\sigma_r}^2$ is also given by an exponential law,

$${\sigma_r}^2(R) = {\sigma_0}^2 \exp(-R/h), \tag{2}$$

where σ_0 is the radial velocity dispersion at the center. We choose parameters such that the typical Toomre (1964) Q parameter is about 1.3, and the models are globally unstable to the formation of bars.

For simplicity, the black holes are handled as external fields, and their potentials, $\phi_{\rm BH}$, are represented by a softened point-mass using a spline-kernel (Hernquist, Katz 1989), given by

$$\phi_{\rm BH}(R) = -GM_\bullet(t) f(R), \tag{3}$$

where G is the gravitational constant, and $M_\bullet(t)$ is the BH mass at time t. The function $f(R)$ is expressed by

$$f(R) = \begin{cases} -(2/\epsilon_{\rm BH})\left[(1/3)u^2 - (3/20)u^4 \right. \\ \quad \left. +(1/20)u^5\right] + 7/(5\epsilon_{\rm BH}), & 0 \le u < 1, \\ -1/(15R) - (1/\epsilon_{\rm BH})\left[(4/3)u^2 - u^3 \right. \\ \quad \left. +(3/10)u^4 - (1/30)u^5\right] \\ \quad +8/(5\epsilon_{\rm BH}), & 1 \le u \le 2, \\ 1/R, & u > 2, \end{cases} \tag{4}$$

where $u = R/\epsilon_{\rm BH}$, and $\epsilon_{\rm BH}$ is the scale-length of the BH potential. As an advantage of this form, we can represent BHs as being close to a point mass by choosing $\epsilon_{\rm BH}$ as small as possible, because equation (4) shows that such a spline-softened potential reduces to a pure Newtonian potential when the distance from the center is larger than $2\epsilon_{\rm BH}$.

The BH is added at $t = t_{\rm BH}$, long after the bar instability has occurred, and its mass grows slowly from 0 to $M_{\rm BH}$ as follows:

$$M_\bullet(t) = \begin{cases} M_{\rm BH}\tau^2(3-2\tau), & 0 \le \tau \le 1, \\ M_{\rm BH}, & \tau > 1, \end{cases} \tag{5}$$

where $\tau = (t - t_{\rm BH})/t_{\rm grow}$, and $t_{\rm grow}$ is the time for the BH to grow to its full amplitude $M_{\rm BH}$. Thus, the BH is made to grow adiabatically by taking $t_{\rm grow}$ to be sufficiently long. In our dimensionless system of units, described below, $t_{\rm BH}$ is set to be 100, and $t_{\rm grow}$ is chosen to be 50 (see appendix 1). Here, we consider cases with $M_{\rm BH}/M =$ 0.001, 0.002, 0.003, 0.005, 0.007, and 0.01, where M is the total mass of the disk. For these BH masses, we use $\epsilon_{\rm BH} = 0.01h$ unless otherwise specified. This value of $\epsilon_{\rm BH}$ may be compared with a radius of $R_{\rm BH}$ within which the disk mass is equal to the full BH mass $M_{\rm BH}$. Obviously, $R_{\rm BH}$ increases monotonically with increasing $M_{\rm BH}$. For example, $R_{\rm BH}/h = 0.045$ for $M_{\rm BH}/M = 0.001$, and $R_{\rm BH}/h = 0.10$ for $M_{\rm BH}/M = 0.005$. Consequently, $\epsilon_{\rm BH}$ is at least one-tenth of $R_{\rm BH}$ for $M_{\rm BH}/M \ge 0.005$, and it is still less than one-fourth of $R_{\rm BH}$, even for $M_{\rm BH}/M = 0.001$. Thus, our choice of $\epsilon_{\rm BH}$ is sufficiently small to model BHs as point masses. An example of the effect of $\epsilon_{\rm BH}$ on the evolution of the bar amplitude is shown in appendix 2.

Once the disks have been realized with particles, we evolve them forward in time using a self-consistent field (SCF) method, as termed by Hernquist and Ostriker (1992), for which no explicit softening of gravitational forces is needed. (We note, however, that these codes are still subject to two-body relaxation owing to

discreteness effects, as shown by Hernquist and Barnes 1990.) In the SCF code, we adopt Aoki and Iye's (1978) basis set, which is appropriate for systems that are flat and have no vertical extent. In a dimensionless system of units, the density basis functions, μ_{nm}, and the potential basis functions, Φ_{nm}, are expressed, respectively, by

$$\mu_{nm}(\boldsymbol{R}) = \frac{2n+1}{2\pi}\left(\frac{1-\xi}{2}\right)^{3/2} P_{nm}(\xi)\exp(im\theta) \qquad (6)$$

and

$$\Phi_{nm}(\boldsymbol{R}) = -\left(\frac{1-\xi}{2}\right)^{1/2} P_{nm}(\xi)\exp(im\theta), \qquad (7)$$

where $\boldsymbol{R} = (R,\theta)$ is the position vector, the P_{nm} are Legendre functions, and n and m ($n \geq m$) are the radial and azimuthal "quantum numbers", respectively. In particular, positive values of m correspond to the number of arms in spiral patterns. In equations (6) and (7), the radial transformation

$$\xi = \frac{R^2-1}{R^2+1} \qquad (8)$$

is used. With these basis functions (μ_{nm}, Φ_{nm}), each pair of which satisfies Poisson's equation, the density and potential of the system can be expanded, respectively, as

$$\mu(\boldsymbol{R}) = \sum_{nm} A_{nm}(t)\mu_{nm}(\boldsymbol{R}) \qquad (9)$$

and

$$\Phi(\boldsymbol{R}) = \sum_{nm} A_{nm}(t)\Phi_{nm}(\boldsymbol{R}). \qquad (10)$$

The simulation procedure using an SCF method is described by Hernquist and Ostriker (1992) and by Hozumi (1997).

The amplitude of the (n, m)-mode at time t is calculated from the absolute value of the expansion coefficients, $|A_{nm}(t)|$. If a spatially constant shape, like a bar pattern, emerges in a model disk, $A_{nm}(t)$ will be proportional to $\exp(-i\omega t)$, where ω is the complex eigenfrequency, and $\mathrm{Im}(\omega)$ will be almost zero in a nonlinear regime. Thus, the pattern speed for the (n,m)-mode is obtained from $\mathrm{Re}(\omega)/m$. In evaluating bar amplitudes, we pay attention only to the fastest growing mode with $(n,m) = (2,2)$, because it will finally dominate the disk by overwhelming other modes in a linear regime. Accordingly, we use $|A_{22}(t)|$ to measure the bar amplitude at time t.

We employ $N = 131072$ particles of equal mass. The equations of motion are integrated in Cartesian coordinates using a time-centered leapfrog algorithm (e.g., Press et al. 1986). A system of units is taken such that $G = M = h = 1$. If these units are scaled to physical values appropriate for the Milky Way, i.e., $h = 3.5$ kpc and $M = 5.6\times10^{10} M_\odot$, the units of time and velocity are 1.31×10^7 yr and 262 km s^{-1}, respectively.

In SCF simulations, the maximum numbers of radial and azimuthal expansion coefficients, $n_{\max}$ and $m_{\max}$, must be specified. It is desirable to include as many expansion terms as possible to trace the evolution of small-scale structures. Then, we choose $m_{\max} = 12$, for which only even m-values are used to avoid an appreciable difference between the center of the bar and the position of the BH owing to asymmetric features that would originate from odd-armed modes. For this value of $m_{\max}$, we adopt $n_{\max} = 24$ from convergence tests for determining $n_{\max}$. Some test experiments with larger $n_{\max}$ and $m_{\max}$ were found to give very similar results.

We first run a simulation until a bar has developed fully in the disk, and then continue the evolution, after growing a BH according to equation (5). We use a time step $\Delta t = 0.05$ when there is no BH. At time $t_{\rm BH} = 100$ when the bar has reached a nearly steady state, we add a BH at the center of the disk. After $t_{\rm BH} = 100$, we employ $\Delta t = 0.01$ for the model with $M_{\rm BH} = 0.001$, and $\Delta t = 0.005$ for the rest of the models. These choices of time step were determined by performing simulations with different values of Δt and requiring that the results of the integrations no longer depended on Δt. For these time steps chosen, the total energy of the system after the full growth of the BH was, in all cases, conserved to better than four significant figures.

3. Results

3.1. *Evolution of Bars*

In figure 1, we show the time evolution of the density distributions after the BH is added at the center of the disk for $M_{\rm BH} = 0, 0.001, 0.003, 0.005$, and 0.01. From this figure, we can see that the bar shape remains practically unchanged to the end of the run for $M_{\rm BH} = 0.001$, although the bar pattern speed is affected to some degree, as is apparent from comparing the direction of the bar major axes at corresponding times between this model and that without a black hole. Once the BH mass exceeds 0.3% of the disk mass, the bar shape becomes rounder with time; for $M_{\rm BH} = 0.003$, the bar has finally become round in a large measure, but it appears still slightly elongated at $t = 400$, while for $M_{\rm BH} = 0.005$ and $M_{\rm BH} = 0.01$, the bar has been almost completely destroyed at $t = 400$. This behavior of the bar shape for BH masses is illustrated clearly in figure 2, which shows the axis ratio of the bars at the end of the simulations as a function of radius, along with the axis ratio profile of the bar at $t = 100$. Here, we determined the axis ratios of the bars by calculating the principal moment of inertia tensor for particles included in a specified radius, and used this information to derive the axis ratio at that radius. We are reassured from figure 2 that BHs whose masses are at least larger than 0.005 can destroy the bar by the end of the simulations, because the axis ratios of these bars are roughly larger than 0.9 at all radii, while a BH with $M_{\rm BH} = 0.003$ can make the bar rounder but it cannot eliminate the bar thoroughly by $t = 400$.

Next, we also notice from figure 1 that the deformation of the bar into a rounder shape proceeds gradually with time. To be more specific about the change in bar

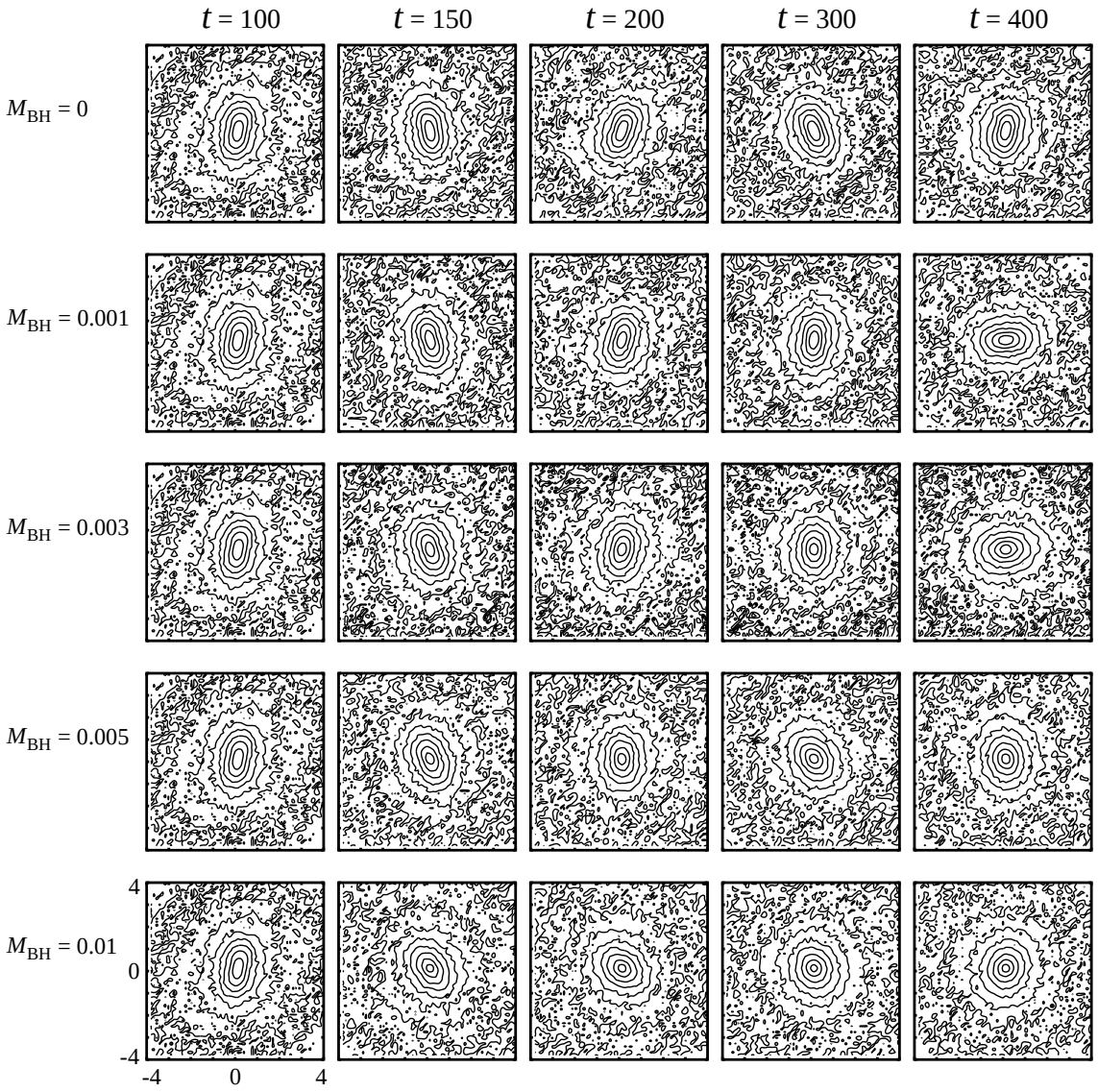

Fig. 1. Time evolution of the density contours in barred structures after the addition of black holes with $M_{\rm BH} = 0$, 0.001, 0.003, 0.005, and 0.01. The contours are drawn at the 90, 80, 70, $\cdots$, and 20% levels of the peak amplitude on logarithmic scales. Black hole growth commenced at $t = 100$, and was completed at $t = 150$. The bar patterns rotate counterclockwise.

strength, the time evolution of the bar amplitude for each BH mass is shown in figure 3. This figure demonstrates that after the BH grows to its full mass ($t \geq 150$), the bar amplitude decreases nearly exponentially with time, and that the rate at which the bar amplitude decays increases with increasing BH mass. In particular, it is to be noticed that only slight as it is, even the bar amplitude for $M_{\rm BH} = 0.001$ decreases at a higher rate than that for the model without a BH. As an example, figure 4 presents the time evolution of the bar axis ratio profile for $M_{\rm BH} = 0.005$, and shows that the axis ratio at each radius increases mildly in the bar region as time proceeds. Thus, the bar is made gradually rounder with time by a massive central BH.

As found from figure 3, the amplitude of the bar decays nearly exponentially with time, $\sim \exp(-t/\tau_{\rm decay})$, once the BH is fully developed. From the decline of $\ln|A_{22}|$ with time, we can estimate decay times as e-folding times, $\tau_{\rm decay}$. In the computation of $\tau_{\rm decay}$, the period from $t = 350$ to $t = 400$ was used. Then, these e-folding times are plotted against $M_{\rm BH}$ in figure 5, in which the unit time is converted to gigayears by adjusting the physical values to those of the Milky Way. This figure indicates that the decay time scales for $M_{\rm BH} \gtrsim 0.002$ are smaller than the inferred ages of disk galaxies. Therefore, we expect that a black hole with a mass as small as 0.2% of the disk mass could substantially deform a bar into an almost round shape, and in some cases, could dissolve a bar, provided that the bar formed at around the same time as the disk. However, in reality, the exponential decay in the bar amplitude might not continue until the present time, so that the required lower bound of the BH mass could be higher than 0.2% of the disk mass.

For the results described above, the scale-length of the

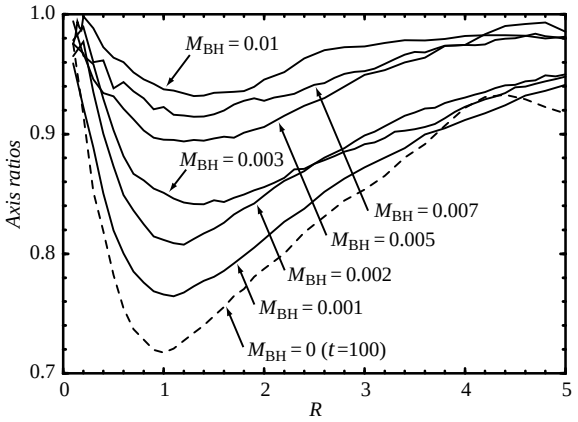

Fig. 2. Axis ratios of bars as a function of radius at the end of the simulations ($t = 400$) for each black hole mass model. In the case without a black hole, the axis ratios are calculated at $t = 100$ just before the addition of a black hole.

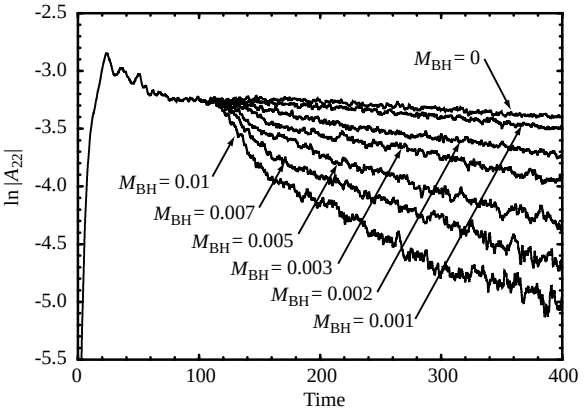

Fig. 3. Time evolution of the bar amplitude, $|A_{22}|$, for each black hole mass model, along with the model without a black hole. A black hole was added at $t = 100$, and was fully developed at $t = 150$.

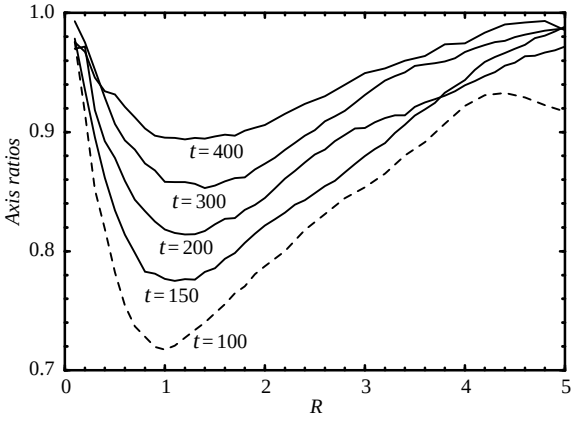

Fig. 4. Time evolution of bar axis ratios as a function of radius for $M_{BH} = 0.005$. Black hole growth began at $t = 100$ and was completed at $t = 150$.

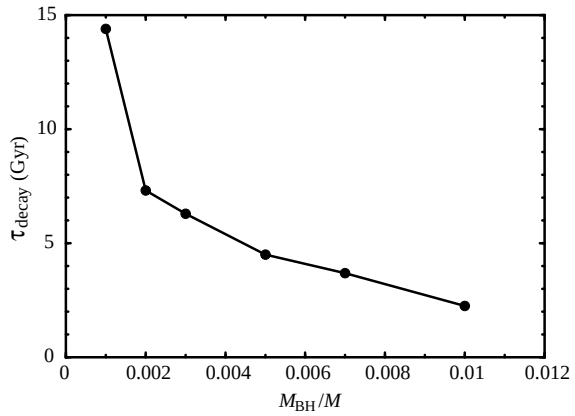

Fig. 5. Decay time scale of the bar amplitude as a function of black hole mass, provided that the bar amplitude is proportional to $\exp(-t/\tau_{decay})$ after the full growth of a black hole. The decay time scales are estimated from the change in bar amplitude between $t = 350$ and $t = 400$, and they are converted to the physical times on the basis of the values appropriate for the Milky Way.

BHs is $\epsilon_{BH} = 0.01$, that is, 35 pc when converted to physical units. In real barred galaxies, sufficiently dense concentrations of gas with masses of 10^7–$10^9 M_\odot$ are often found in central regions (Sakamoto et al. 1999; Regan et al. 2001). Then, we examined the influence of such mass concentrations by selecting $\epsilon_{BH} = 0.03$, that is, ~ 100 pc, a likely smallest size for them. The mass of a concentration corresponding to M_{BH} is taken to be 0.005. The parameters necessary for the simulation are the same as those employed for the case with $M_{BH} = 0.005$ except for ϵ_{BH}. From the results shown in figure 6, we find that a dense central concentration with a mass 0.5% of the disk mass can make a bar rounder and can reduce the bar amplitude to a certain degree, but that the bar still survives until the end of the run. Indeed, we have obtained about 1.14×10^{10} yr as an e-folding decay time scale in this case.

3.2. Structural Properties of Bar-Dissolved Galaxies

In figure 7, we show the final surface density profiles of the models for which the bar has been made significantly round, that is, for $M_{BH} = 0.005$, 0.007, and 0.01, together with those of the disk at $t = 0$ and $t = 100$. Since the bar-dissolved models are not perfectly axisymmetric even at the end of the simulations (see figure 2), all the surface density profiles are constructed along the major axis by selecting the particles whose positions are involved in a small angle from the origin with respect to the major axis. The initial exponential surface density distribution is converted to a more centrally concentrated one by the bar instability. In particular, the steep rise of the surface density is prominent in the region $R \lesssim 2$. From a comparison between the density contours in figure 1 and the surface density profiles in figure 7, we find that $R \sim 2$ corresponds to around the end of the bar along the major axis. The introduction of a BH at the center of the disk does not change the surface density distribution within the bar region, $R \lesssim 2$, substantially from that at $t = 100$,

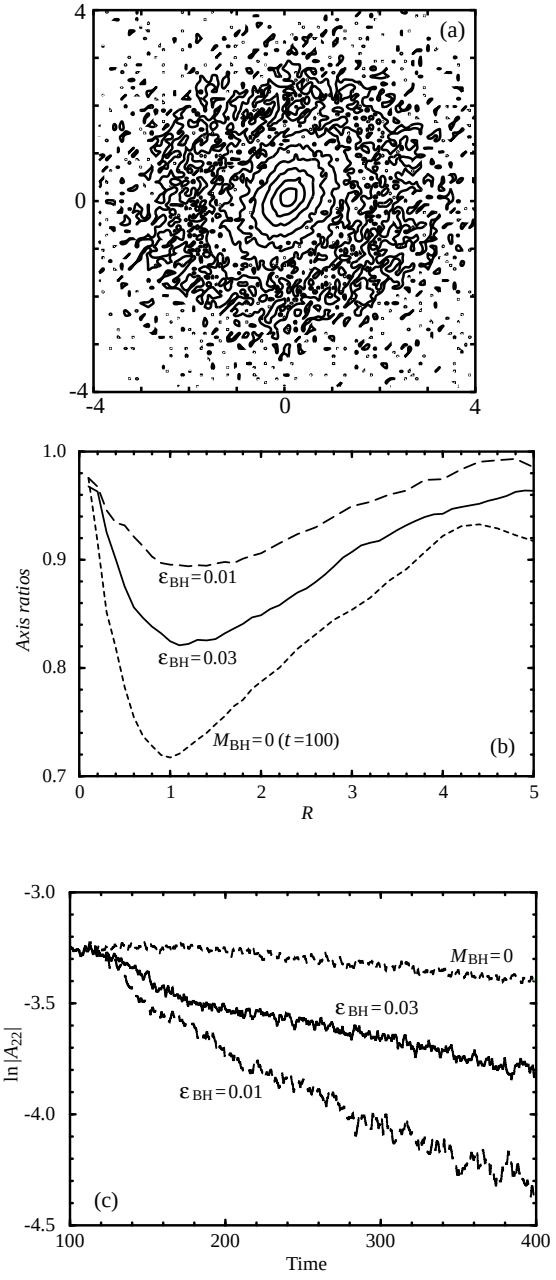

Fig. 6. Density contour (a), axis ratio profile (b), at the end of the run, $t = 400$, and time evolution of the bar amplitude (c), for $M_{\rm BH} = 0.005$ with $\epsilon_{\rm BH} = 0.03$. In this instance, $M_{\rm BH}$ can be considered to be the mass of a dense central concentration. As a comparison, the following cases are also shown: (b) the axis ratio profiles for $M_{\rm BH} = 0.005$ with $\epsilon_{\rm BH} = 0.01$ at $t = 400$ and for a model without a black hole at $t = 100$, and (c) the time evolution of the bar amplitudes for $M_{\rm BH} = 0.005$ with $\epsilon_{\rm BH} = 0.01$ and for a model without a black hole.

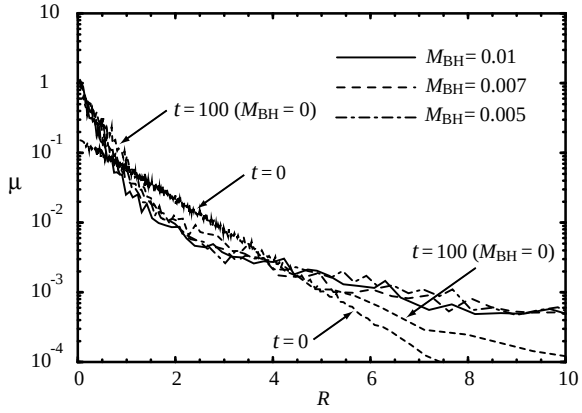

Fig. 7. Surface density profiles at the end of the runs, $t = 400$, for the bar-dissolved models. The lines denoted by $t = 0$ and $t = 100$ show the surface density profile of the initial model, and that just before adding a black hole, respectively.

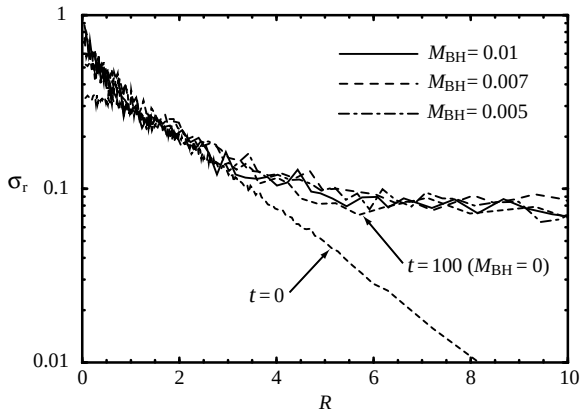

Fig. 8. Radial velocity dispersion profiles at the end of the runs, $t = 400$, for the bar-dissolved models. The lines denoted by $t = 0$ and $t = 100$ show the radial velocity dispersion profile of the initial model, and that just before adding a black hole, respectively.

regardless of the BH mass, although the surface density becomes very high at very small radii owing to the presence of the BH. When we neglect a slight difference in the surface density distributions at $t = 400$ for these three BH masses, we can still roughly fit them with an exponential law outside $R \sim 3$.

In figure 8, we show the final radial velocity dispersion profiles of the models with $M_{\rm BH} = 0.005, 0.007$, and 0.01, together with those of the disk at the beginning and at $t = 100$. Here, $\sigma_{\rm r}$ is calculated along the major axis, as is done for the surface density. This figure indicates that because of the bar instability, $\sigma_{\rm r}$ increases greatly from $t = 0$ to $t = 100$, except in the region around $R \sim 2$, while the final distributions of $\sigma_{\rm r}$ are very similar to one another, irrespective of the BH masses. Like the surface density profiles, the existence of the bar produces a bend in $\sigma_{\rm r}$ at around the end of the bar, $R \sim 2$, inside which $\sigma_{\rm r}$ rises steeply down to the center. However, the subsequent evolution after the addition of a BH ends up with only a slight increase in $\sigma_{\rm r}$ at all radii, although the increase in $\sigma_{\rm r}$ is

rather large at very small radii where the BH dominates the motions of stars. This means that the bar dissolution process hardly heats the disk, as compared to the bar instability. As found from figure 8, the σ_r distribution of the disk that has suffered the bar instability shows an exponential profile at $R \gtrsim 4$. Therefore, no practical change in the σ_r distribution through the process of bar dissolution implies that the σ_r distributions of the bar-dissolved galaxies are also represented by an exponential law at corresponding radii.

Assuming that both the surface density and radial velocity dispersion profiles can be approximated by exponential laws at $R \gtrsim 4$, we can obtain a relation between the two quantities. As can be seen from figures 7 and 8, the difference in the surface density, μ, and the radial velocity dispersion, σ_r, among the BH models is very small from $R \sim 4$ to $R \sim 10$. We find that in this region, $\mu \propto \exp(-0.24R)$ and ${\sigma_r}^2 \propto \exp(-0.12R)$. Consequently, ${\sigma_r}^2$ is proportional to $\mu^{0.5}$, unlike the relation for our Galaxy in which ${\sigma_r}^2 \propto \mu$ holds (van der Kruit, Searle 1981; Lewis, Freeman 1989). In particular, we see that the exponential scale-length of the bar-dissolved disks becomes about four-times as large as that of the initial disk.

3.3. Surfaces of Section

Surfaces of section (SOSs) will give a clue to the bar dissolution mechanism. We construct SOSs in a frame rotating with a bar pattern speed, Ω_b, in which the bar is placed so that its major axis is aligned with the x-axis. For a given value of the Jacobi constant H, orbits are computed for stars starting on the y-axis with $\dot{y} = 0$ by numerically integrating the equations of motion. In so doing, we use the expansion coefficients $A_{nm}(t)$ of the SCF simulations in order to obtain accelerations at each position of a star. Then, SOSs are built up by saving $(y, \dot{y})$ values every time the star crosses the bar minor axis with $\dot{x} < 0$. It thus follows that the right-hand side of the SOS plots represents crossings in the prograde sense, while the left-hand side corresponds to those in the retrograde sense.

Figures 9 and 10 show the evolution of SOSs for six values of the Jacobi constant for $M_{BH} = 0$ and those for $M_{BH} = 0.005$, respectively. In figure 9a, we plot the SOSs for the disk, which has suffered the bar instability, at $t = 100$ just before adding a BH. These SOSs have evolved through those at $t = 150$ (figure 9b) into those at $t = 400$ (figure 9c). When a BH with $M_{BH} = 0.005$ is added at $t = 100$, the SOSs at $t = 100$ (figure 10a) have turned into those at $t = 150$ when the BH has grown up completely (figure 10b), and they have resulted in those at $t = 400$ (figure 10c). Here, notice that the SOSs in figure 10a are exactly identical to those in figure 9a. For a given value of H, a particle can reach the limiting distance y_0 on the bar minor axis. Following Norman et al. (1996), we denote this value of H by $H(0, y_0)$.

At $t = 100$ when there is no black hole, we find, as nested invariant curves, the B family of direct orbits (x_1 orbits) on the right-hand side of the SOS plots shown in figure 9a. The orbits of this family are the loop orbits that are believed to sustain bars. The subsequent evolution of the bar without the influence of a BH does not change the basic properties of SOS plots. Figures 9b and 9c demonstrate that nested invariant curves are still maintained. As often discussed in the literature (Hasan, Norman 1990; Norman et al. 1996; Shen, Sellwood 2004), the retrograde orbits represented by the invariant curves on the left-hand side of the SOS plots are insignificant for supporting bars owing to the low population of stars.

The addition of a black hole changes SOSs, as found from figures 10b and 10c. The black hole can make some orbits of the major family stochastic, so that the outer invariant curves of the major family disappear. Consequently, the SOSs are occupied by stars whose orbits are determined by the energy integral H alone. As the value of H becomes smaller, stochastic regions prevail more and more in the SOSs. The evolution of the SOSs shown in figure 10 is quite similar to that presented in figure 11 of Shen and Sellwood (2004), although they constructed SOSs by projecting three-dimensional orbits onto the mid-plane of the disk: many bar-supporting orbits become chaotic during the phase of the BH growth as seen from figure 10b, and subsequently, the secular settlement of the global potential of the system allows x_1 orbits to exist again because the bar has been removed incompletely as found from figure 4. This behavior in the SOS plots suggests that the decay in the bar amplitude and, in some cases, the bar dissolution are caused by a decrease in the population of bar-supporting orbits owing to chaos induced by the presence of a black hole.

4. Discussion

We have shown that a massive central BH can dissolve a bar within a relatively short time scale if the BH is as massive as about 0.5% of the disk mass. This finding indicates that the minimum BH mass required for bar dissolution would be on the order of $10^{8.5} M_\odot$ for a typical disk galaxy. Furthermore, we have also shown that even a BH with 0.3% of the disk mass can deform a bar into a round shape in a short period of time. Our minimum BH mass is close to the largest BH masses inferred in nearby spiral galaxies, but not abnormally large, and still within the range of the estimated BH masses from observations (Kormendy, Gebhardt 2001; Tremaine et al. 2002; Marconi, Hunt 2003). In fact, the Sa galaxy NGC 4594 is thought to contain a central BH with a mass of $\sim 10^9 M_\odot$ (Kormendy 1988; Marconi, Hunt 2003). Therefore, although this bar dissolution cannot be a frequent event, it could occur in the real Universe, and some fraction of bars in real barred galaxies could be made rounder to some extent in the course of the Hubble time, even if they are not completely dissolved.

Our minimum BH mass necessary for bar dissolution is about an order of magnitude smaller than that obtained by Norman et al. (1996) and that by Shen and Sellwood (2004). Our simulations differ from these in several respects, and we do not know which difference is most responsible for our lower value of this BH mass. The way of modeling a BH is indeed different between Norman et

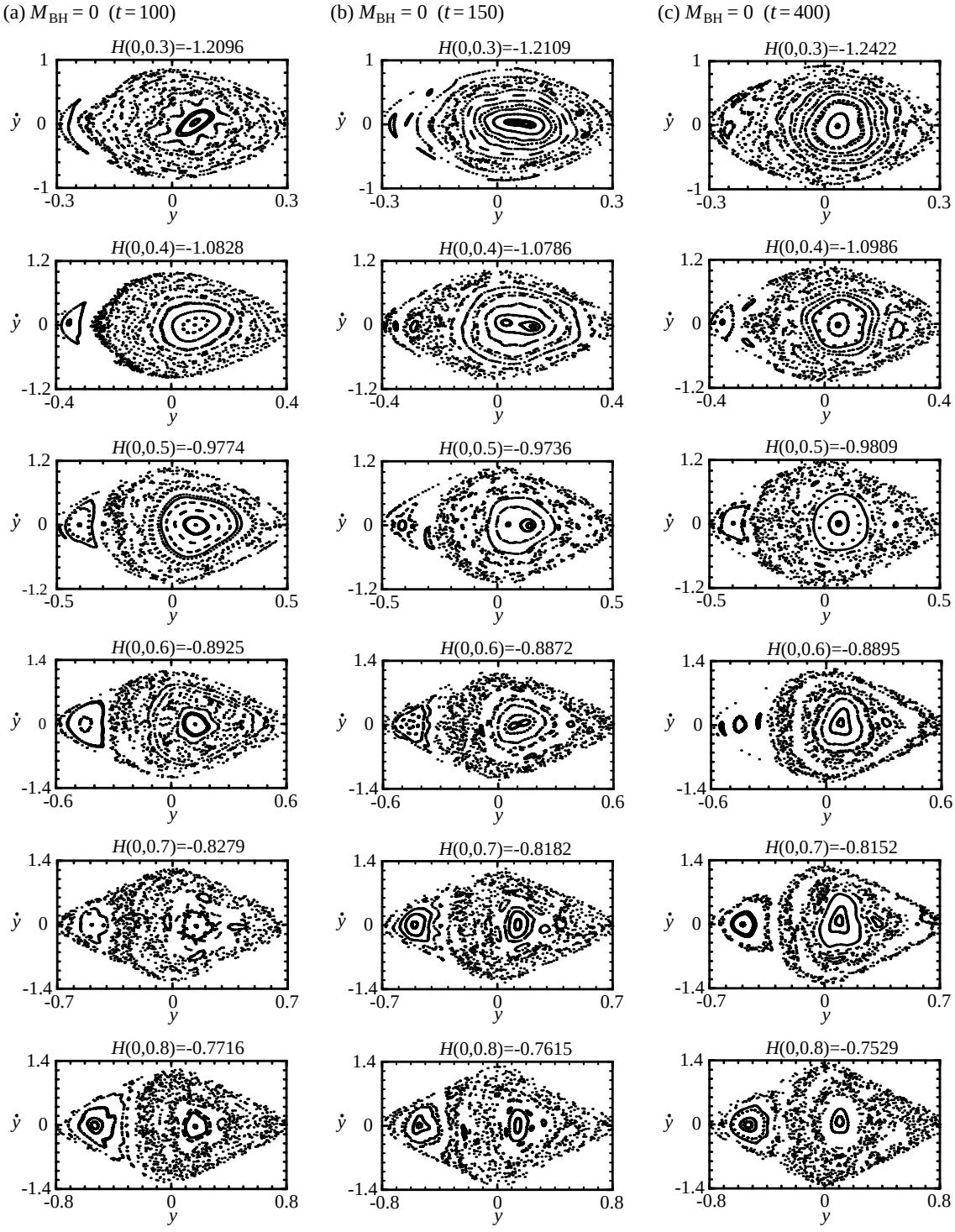

Fig. 9. Surfaces of section (SOS) for six selected values of the Jacobi constant, $H(0, y_0)$, without a black hole, for which a particle can reach the limiting distance, y_0, on the bar minor axis. Shown are (a) SOSs at $t = 100$, (b) SOSs at $t = 150$, and (c) SOSs at $t = 400$.

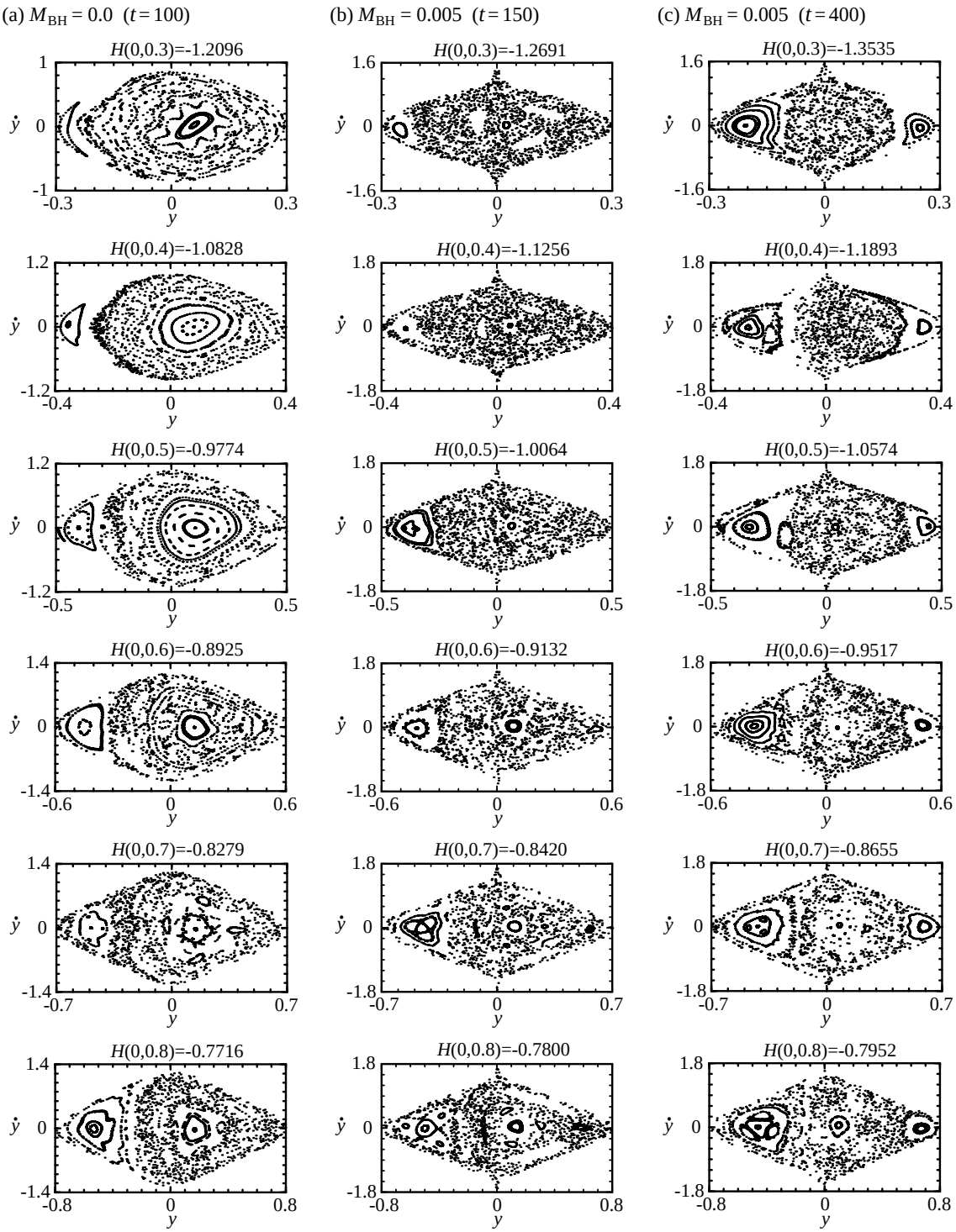

Fig. 10. Same as in figure 9 but in the case of a BH with $M_{\rm BH} = 0.005$ (a) at $t = 100$ just when the BH growth has commenced, (b) at $t = 150$ just when the BH growth has been completed, and (c) at $t = 400$. Notice that the SOS plots at $t = 100$ are exactly identical to those for the model without a BH in figure 9.

al.'s (1996) simulations and ours, while ours is similar to that in Shen and Sellwood's (2004) simulations. This suggests that the difference in the minimum BH mass does not originate primarily from the difference in the BH model. It is conceivable that the important difference arises from the disk models: Norman et al. (1996) and Shen and Sellwood (2004) adopted Kuzmin–Toomre disks, while we have employed exponential disks. The latter are significantly more centrally concentrated than the former. As a result, it is likely that a relatively larger fraction of the stars supporting the bars in our simulations pass sufficiently near that central mass to be strongly perturbed by it. Therefore, the impact of a central BH is considered to be stronger in exponential disks than in Kuzmin–Toomre disks. This reasoning is supported by the finding of Shen and Sellwood (2004) that after the orbits sustaining a bar with lower energies are made chaotic, those with higher energies follow (see the discussion of the mechanism below). Of course, we should compare the density distributions of bars rather than those of disks to estimate the true influence of a BH. Nevertheless, it is quite likely that more centrally concentrated bars could be formed in more centrally concentrated disks by the bar instability.

Very recently, in relation to the efficient destruction of bars in exponential disks argued above, Athanassoula, Lambert, and Dehnen (2005) investigated bar destruction due to central mass concentrations by employing exponential disks in surface density with live halos in three-dimensional configurations. In their simulations, the galaxy models were divided into two types: one had a small core halo that was more massive in the central parts, and thus denoted as MH-type; the other had a large core halo that was less massive in the central parts, and thus termed MD-type, which stands for massive disk type (also see Athanassoula and Misiriotis 2002). They then demonstrated that the minimum BH mass necessary for bar destruction is at least about 5% of the disk mass, and that the BH mass required for bar destruction is smaller for MD-type models than for MH-type models. Although they adopted exponential disks, their minimum BH mass was about an order of magnitude larger than that found by us. They infer that our adopted time step could be rather large, perhaps enough to result in a spuriously damaging effect on the bar. In this regard, we carried out an additional simulation (not presented here) for $M_{\rm BH} = 0.01$ with $\Delta t = 0.001$, and found that the evolution of the bar amplitude is very similar to that shown in figure 3. If we are allowed to extrapolate their results despite the fact that we used a two-dimensional disk, our disk model, which has no halo component, would correspond to a limiting case of their MD-type models, and so, the minimum BH mass could be smaller than that obtained by them. Unfortunately, we cannot evaluate to what degree the BH mass is reduced for pure disk models at this stage. In addition, there are some other differences between their simulations and ours, except for the geometry (their simulations are three-dimensional, while ours are two-dimensional), so that the exact reason for the difference in the minimum BH mass should be further investigated. As suggested in their paper, the orbital contents of the bars used in both simulations could give us a clue to the degree of robustness or fragility of the bars under the influence of massive central BHs.

In figure 5, we have shown that the e-folding decay time of the bar amplitude, $\tau_{\rm decay}$, decreases with increasing BH mass. We infer that $\tau_{\rm decay}$ asymptotes to zero as $M_{\rm BH}$ approaches infinity, and that $\tau_{\rm decay}$ goes to infinity as $M_{\rm BH}$ approaches zero. Therefore, the relation between $\tau_{\rm decay}$ and $M_{\rm BH}$ will be represented by $\tau_{\rm decay} \propto {M_{\rm BH}}^{\alpha}$, where α is negative. A least-squares fit to our results gives $\alpha = -0.71$, which roughly suggests that $\tau_{\rm decay}$ is inversely proportional to $M_{\rm BH}$. However, this value of α will depend on the disk structure such as density and velocity distributions.

We may be underestimating the response of a bar by softening the potential of the BH and by forcing it to remain stationary at the center of the disk. In reality, a BH near the center of a galaxy would generate a potential that is essentially that of a point mass, and would "wander" about the origin as it achieves equipartition with the background stars (Quinlan, Hernquist 1997; Chatterjee et al. 2002a, b), possibly enhancing the rate at which a bar would be destroyed. Taking into account this black hole "wandering", the minimum BH mass might be further reduced. (Note that the BH wandering is caused by the same discreteness effect that produces relaxation in SCF codes.) In addition, we hold the softening length fixed as we vary the black hole mass, for simplicity. Since this way of modeling black holes means that BHs with smaller masses are softened more loosely, the impact of a BH upon destroying a bar is considered to be weaker for smaller BH masses. In appendix 2, we have demonstrated that the bar amplitude can be lowered more effectively by halving the softening length, $\epsilon_{\rm BH}$, of a BH with $M_{\rm BH} = 0.001$, although the decay time scale for $\epsilon_{\rm BH} = 0.005$ is comparable to that for $\epsilon_{\rm BH} = 0.01$. This result indicates that we do not capture all of those large-angle scatterings by the black hole which would exist if it were a point mass. In this sense, the minimum BH mass that we have obtained here is an upper bound for bar destruction, because we underestimate the effect of small black holes, although the degree of missing such large-angle scatterings is not so high for that small BH mass, as also shown in appendix 2. Therefore, this fact only strengthens our conclusion that relatively small black holes can affect bars.

From an observational point of view, Das et al. (2003) have obtained an inverse correlation between bar ellipticity and central mass concentration. On the basis of this correlation, they suggest that the mass concentration may eventually dissolve a bar. Since their definition of mass concentration is the ratio of the dynamical mass within the bulge to that within the bar radius, the correlation that they have found may not be direct evidence for the occurrence of bar dissolution caused by dense concentrations of gas in the central regions of disk galaxies. In addition, in our case where the scale-length of a mass concentration corresponds to about 100 pc, a bar cannot be destroyed, even though the mass of the concentration

amounts to about $10^{8.5} M_{\odot}$. Similar results are shown by Shen and Sellwood (2004) with an extensive study of the compactness of central mass concentrations. Therefore, the correlation obtained by Das et al. (2003) may be a manifestation of a variety of the bars formed by the bar instability that is affected by bulges with a wide range of the mass and scale-length.

Very recent observations indicate that the bar fraction is constant out to a redshift of $z \sim 1$ (Sheth et al. 2003; Elmegreen et al. 2004; Jogee et al. 2004). Then, Elmegreen et al. (2004) have concluded that most bars do not dissolve within the Hubble time. Their conclusion is not necessarily inconsistent with our results, as we have stated that bar dissolution can occur rarely in the history of the Universe. However, if some galaxies experience bar dissolution, we could discriminate between a priori non-barred galaxies and bar-dissolved galaxies from the viewpoint of structural properties such as surface density and radial velocity dispersion. Although bar-dissolved galaxies show an exponential profile in surface density, their exponential scale-length would be substantially, say about four times, larger than those of non-barred galaxies by birth. This means that the scale-length of bar-dissolved galaxies could amount to about 14 kpc. In addition, we have found that the bar dissolution process does not practically heat the disk. As a result, the distribution of ${\sigma_{\rm r}}^2$ for bar-dissolved galaxies is determined by the bar instability, and shows shallower dependence on μ, like ${\sigma_{\rm r}}^2 \propto \mu^{0.5}$, than that for our Galaxy, in which ${\sigma_{\rm r}}^2 \propto \mu$ holds (van der Kruit, Searle 1981; Lewis, Freeman 1989). Thus, the bar-dissolved disks would have a large $\sigma_{\rm r}$ at large distances as shown in figure 8. Taking into account these characteristics of bar-dissolved galaxies, we should mention some simulations in which bar dissolution is driven by dense central mass concentrations (Friedli, Benz 1993; Berentzen et al. 1998; Bournaud, Combes 2002). As we have already argued, this kind of bar dissolution might be implausible in reality. Even though such a phenomenon could be realized, the end-products would not look like genuine non-barred galaxies because of their large exponential scale-lengths and large radial velocity dispersion distributions.

Previous studies (Hasan, Norman 1990; Hasan et al. 1993; Norman et al. 1996; Shen, Sellwood 2004) have revealed from SOS plots that after the introduction of a BH, a large fraction of the loop orbits that probably support a bar become chaotic. In our cases, similar SOS plots have been obtained as presented in figure 10. Thus, we can rely on a picture that the bar dissolution studied here originates from that chaotic behavior in bar-supporting orbits which is excited by the growth of a central BH. Consequently, the disappearance of these loop orbits promotes the erosion of a bar. In the process of bar dissolution, Norman et al. (1996) found that the bar amplitude decreased suddenly after the full growth of a BH, and argued that the interpretation based on chaotic behavior in orbits accounts for this abrupt destruction of a bar. On the other hand, our results indicate that even though the origin is chaos, a bar dissolves gradually with time. This difference in the rate of dissolving a bar might be caused by the difference in the way of introducing a BH: Norman et al. (1996) reduced the scale-length of a central mass concentration to finally build up a BH, while we allowed the BH mass to grow adiabatically.

We have considered only infinitesimally thin disks. This restriction could enhance the influence of a BH on the disk by requiring the orbits of stars to remain in a single plane. However, for now we note that Norman et al. (1996) modeled disks both with and without vertical extent, and did not find a significant difference in the magnitudes of the central mass concentrations required for destroying a bar. Rather, by focusing on two-dimensional disks, we can evaluate, in a sense, the impact of a central BH on a bar alone, because the adoption of three-dimensional disks would lead to a fire-hose instability, which affects their vertical structure and can destroy a bar in some cases (Raha et al. 1991; Debattista et al. 2004; Martinez-Valpuesta, Shlosman 2004).

Conventional N-body methods need the explicit introduction of a softening length, which often casts doubt on how faithful N-body simulation results are to reality. In particular, for cold systems like those galaxy disks studied here in which rotation is dominant, the modification of force fields through a softening length could alter the global dynamics of a disk to a large degree. In fact, Earn and Sellwood (1995) have demonstrated that for an isochrone disk, the growth rate and pattern speed of the fastest growing two-armed mode obtained with their smallest softening length are still about 20% smaller than those derived from linear analysis. On the other hand, if an SCF method is used, the growth rate and pattern speed are in excellent agreement with those predicted by linear theory. In our simulations, we have avoided complications arising from a softening length by adopting an SCF method, so that the estimated minimum BH mass will be close to that which is actually needed to destroy a bar.

5. Conclusions

We examined the damaging impact of massive central BHs on bars formed in two-dimensional exponential disks using N-body simulations. We found that a bar can be completely destroyed in a time much smaller than the Hubble time if the central BH exceeds about 0.5% of the disk mass. This minimum BH mass is on the order of $10^{8.5} M_{\odot}$ for a typical disk galaxy, and so, it is not extremely large as compared with the BH masses suggested by observations. Therefore, the bar dissolution induced by a massive central BH could occur at some unexceptional rate in real barred galaxies. We also found that a bar can be seriously damaged in the Hubble time if the central BH is around 0.3% of the disk mass. Thus, we expect that some fraction of bars in real barred galaxies would have been made round by a central BH. On the other hand, our additional simulation has exemplified the insufficiency for bar destruction caused by dense central mass concentrations because of their extended distribu-

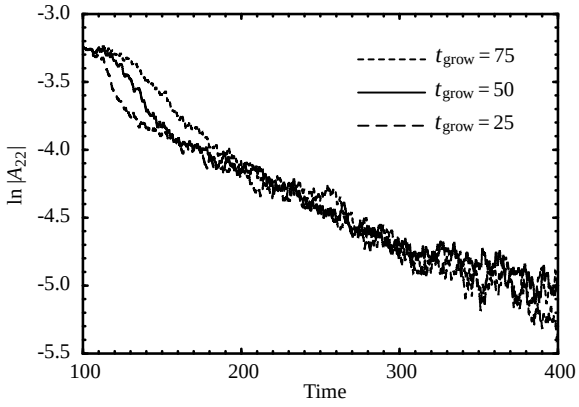

Fig. 11. Time evolution of the bar amplitude, $|A_{22}|$, after the addition of a black hole with $M_{\rm BH} = 0.01$ when the growing time of the black hole mass, $t_{\rm grow}$, is varied.

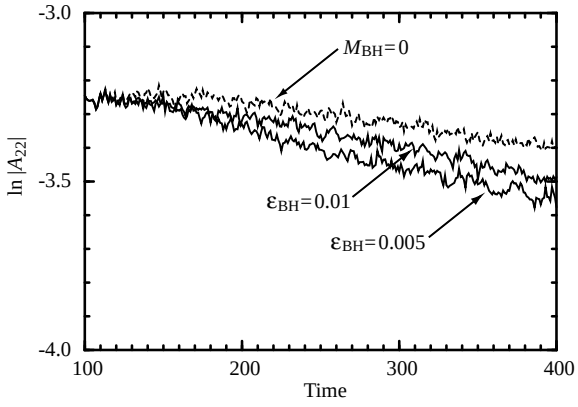

Fig. 12. Time evolution of the bar amplitude, $|A_{22}|$, after the addition of a black hole with $M_{\rm BH} = 0.001$ when the softening length of the black hole, $\epsilon_{\rm BH}$, is varied. Black hole growth was completed at $t = 150$. As a reference, the time evolution of the bar amplitude without adding a black hole is also shown.

tions, even though their masses amount to the minimum BH mass derived here.

We have demonstrated that bar-dissolved galaxies have a large exponential scale-length in surface density and a large radial velocity dispersion profile, although the bar dissolution process hardly heats the disk. In addition, we have shown that the resulting surface density and radial velocity dispersion profiles are related to each other as ${\sigma_{\rm r}}^2 \propto \mu^{1/2}$ unlike the relation for our Galaxy ${\sigma_{\rm r}}^2 \propto \mu$. We thus suggest that these structural properties could be used to discriminate observationally between bar-dissolved galaxies and a priori non-barred galaxies.

Regarding the mechanism of the bar dissolution studied here, the surface-of-section plots strongly indicate that it originates from the conversion of loop orbits into stochastic orbits owing to the influence of a central BH. We have found that the chaotic origin of bar dissolution leads to a gradual erosion of a bar unlike the view that chaos is responsible for a sudden destruction of a bar.

We are grateful to Professor A. Burkert for stimulating discussions. We thank Dr. C. Efthymiopoulos for valuable communications concerning the construction of surfaces of section. Thanks are also due to Professor E. Athanassoula for useful discussions on bar dissolution, and to Dr. R. Jesseit for his critical reading of the original manuscript. We appreciate helpful comments by the anonymous referee. One of the authors (SH) acknowledges University of California, Santa Cruz, and Max-Planck-Institut für Astronomie, Heidelberg for their hospitality, where part of this work was done.

Appendix 1. Growing Time of a Black Hole

We examine how long the growth time of a black hole, $t_{\rm grow}$, should be to ensure adiabaticity. Figure 11 presents the time evolution of the bar amplitude after the addition of a BH with $M_{\rm BH} = 0.01$ for $t_{\rm grow} = 25$,50, and 75. Other simulation parameters are the same as those described in section 2. We can see that these choices of $t_{\rm grow}$ result in a similar evolution of the bar amplitude after the BH has reached its full mass.

In choosing a suitable $t_{\rm grow}$, it is useful to compare the above selected values for $t_{\rm grow}$ with the typical rotation periods of the bars in the simulations, $T_{\rm b}$. To estimate $T_{\rm b}$, the phase angle $\phi_{\rm b}(t)$ of the bar pattern is derived from the phase of the expansion coefficients, $A_{22}(t)$, divided by 2 (the number of arms), as explained in section 2. Thus, the bar rotation period can be calculated from the time derivative of $\phi_{\rm b}(t)$. We obtain $\Omega_{\rm b} = 0.270$ at around $t = 100$ when there was no BH. This means that the bar rotation period is $T_{\rm b} = 2\pi/\Omega_{\rm b} = 23.4$. Consequently, $t_{\rm grow} = 50$ is at least more than twice as long as $T_{\rm b}$, while $t_{\rm grow} = 25$ is comparable to $T_{\rm b}$. In addition, $t_{\rm grow} = 50$ is much longer than the dynamical times of stars near the center of the disk. Therefore, the choice of $t_{\rm grow} = 50$ is reasonable to regard the black hole growth as adiabatic.

Appendix 2. Softening Length of a Black Hole

We consider to what degree the softening length of a black hole, $\epsilon_{\rm BH}$, affects the bar amplitude when the black hole mass is small. Figure 12 shows the time evolution of the bar amplitude after the addition of a BH with $M_{\rm BH} = 0.001$ for $\epsilon_{\rm BH} = 0.005$ and $\epsilon_{\rm BH} = 0.01$. The value of $\epsilon_{\rm BH} = 0.005$ corresponds closely to one-ninth of $R_{\rm BH}$ for $M_{\rm BH} = 0.001$, where $R_{\rm BH}$ is the radius within which the disk contains the assigned $M_{\rm BH}$, as explained in section 2. In the simulation for $\epsilon_{\rm BH} = 0.005$, we adopt $\Delta t = 0.0025$ to ensure that the total energy of the system after the full growth of the BH is conserved to better than four significant figures. The rest of the simulation parameters is the same as those for $\epsilon_{\rm BH} = 0.01$.

We find from figure 12 that the bar amplitude is reduced more effectively for $\epsilon_{\rm BH} = 0.005$ than that for $\epsilon_{\rm BH} = 0.01$ after the full growth of the BH ($t \geq 150$), but that the difference in bar amplitude between the two cases is relatively small. In fact, the final bar amplitudes are 0.0280 and 0.0306 for $\epsilon_{\rm BH} = 0.005$ and $\epsilon_{\rm BH} = 0.01$, respectively.

In addition, the decay time scale, $\tau_{\rm decay}$, is 1.69×10^{10} yr for $\epsilon_{\rm BH} = 0.005$ while it is 1.44×10^{10} yr for $\epsilon_{\rm BH} = 0.01$, if we estimate it from a least-squares fit to the bar amplitude between $t = 350$ and $t = 400$ on the assumption that the bar amplitude decays exponentially.

As the softening length of a BH is smaller, many more large-angle scatterings of stars made by the BH will be captured. In this respect, our choice of $\epsilon_{\rm BH} = 0.01$ for all BH masses will lead to the loss of such large-angle scatterings more seriously for smaller BH masses. As demonstrated from figure 12, this loss is considered to be not so large, even for small BH masses. However, the result demonstrated here indicates that small-mass BHs can have a larger destructing impact upon a bar than those shown in subsection 3.1, if their softening length is made smaller.

References

Aoki, S., & Iye, M. 1978, PASJ, 30, 519
Athanassoula, E., Lambert, J. C., & Dehnen, W. 2005, MNRAS, in press (astro-ph/0507566)
Athanassoula, E., & Misiriotis, A. 2002, MNRAS, 330, 35
Berentzen, I., Heller, C. H., Shlosman, I., & Fricke, K. J. 1998, MNRAS, 300, 49
Bournaud, F., & Combes, F. 2002, A&A, 392, 83
Chatterjee, P., Hernquist, L., & Loeb, A. 2002a, ApJ, 572, 371
Chatterjee, P., Hernquist, L., & Loeb, A. 2002b, Phys. Rev. Lett., 88, 1103
Das, M., Teuben, P. J., Vogel, S. N., Regan, M. W., Sheth, K., Harris, A. I., & Jefferys, W. H. 2003, ApJ, 582, 190
Debattista, V. P., Carollo, C. M., Mayer, L., & Moore, B. 2004, ApJ, 604, L93
Earn, D. J. D., & Sellwood, J. A. 1995, ApJ, 451, 533
Elmegreen, B. G., Elmegreen, D. M., & Hirst, A. C. 2004, ApJ, 612, 191
Eskridge, P. B., et al. 2000, AJ, 119, 536
Freeman, K. C. 1970, ApJ, 160, 811
Friedli, D., & Benz, W. 1993, A&A, 268, 65
Hasan, H., & Norman, C. 1990, ApJ, 361, 69
Hasan, H., Pfenniger, D., & Norman, C. 1993, ApJ, 409, 91
Hernquist, L. 1993, ApJS, 86, 389
Hernquist, L., & Barnes, J. E. 1990, ApJ, 349, 562
Hernquist, L., & Katz, N. 1989, ApJS, 70, 419
Hernquist, L., & Ostriker, J. P. 1992, ApJ, 386, 375
Hozumi, S. 1997, ApJ, 487, 617
Jogee, S., et al. 2004, ApJ, 615, L105
Kormendy, J. 1988, ApJ, 335, 40
Kormendy, J., & Gebhardt, K., 2001, in AIP Conf. Proc., Vol. 586, 20th Texas Symposium on relativistic astrophysics, ed. J. C. Wheeler & H. Martel (New York: American Institute of Physics, Melville), 363
Kuzmin, G. 1956, AZh., 33, 27
Lewis, J. R., & Freeman, K. C. 1989, AJ, 97, 139
Marconi, A., & Hunt, L. K. 2003, ApJ, 589, L21
Martinez-Valpuesta, I., & Shlosman, I. 2004, ApJ, 613, L29
Norman, C. A., Sellwood, J. A., & Hasan, H. 1996, ApJ, 462, 114
Press, W. H., Flannery, B. P., Teukolsky, S. A., & Vetterling, W. T. 1986, in Numerical Recipes: The Art of Scientific Computing (Cambridge: Cambridge University Press), 631
Quinlan, G. D., & Hernquist, L. 1997, New Astron., 2, 533
Raha, N., Sellwood, J. A., James, R. A., & Kahn, F. D. 1991, Nature, 352, 411
Regan, M. W., Thornley, M. D., Helfer, T. T., Sheth, K., Wong, T., Vogel, S. N., Blitz, L., & Bock, D. C.-J. 2001, ApJ, 561, 218
Sakamoto, K., Okumura, S. K., Ishizuki, S., & Scoville, N. Z. 1999, ApJ, 525, 691
Shen, J., & Sellwood, J. A. 2004, ApJ, 604, 614
Sheth, K., Regan, M. W., Scoville, N. Z., & Strubbe, L. E. 2003, ApJ, 592, L13
Toomre, A. 1963, ApJ, 138, 385
Toomre, A. 1964, ApJ, 139, 1217
Tremaine, S., et al. 2002, ApJ, 574, 740
van der Kruit, P. C., & Searle, L. 1981, A&A, 95, 105